4738 *Chem. Mater.* **2009,** *21,* 4738–4745
DOI:10.1021/cm902040v

CHEMISTRY OF MATERIALS
Article

$Ca_3Co_4O_{9-\delta}$: A Thermoelectric Material for SOFC Cathode

K. Nagasawa,[†,‡] S. Daviero-Minaud,[†] N. Preux,[†] A. Rolle,[†] P. Roussel,[†] H. Nakatsugawa,[‡] and O. Mentré*[,†]

[†] *UCCS - Unite de Catalyse et de Chimie du Solide − UMR CNRS 8181, Ecole Nationale Superieure de Chimie de Lille, Batiment C7 − BP.90108, 59652, Villeneuve d'Ascq cedex, France, and* [‡] *Graduate School of Engineering, Yokohama National University, 79-5 Tokiwadai, Hodogaya Word, Yokohama, Kanagawa 240-8501, Japan*

Received July 7, 2009

The misfit compound $[CoO_2][Ca_2CoO_{3-\delta}]_{0.62}$ is well-known for its good potentialities in the field of thermoelectric oxides combining good electronic transport, high Seebeck coefficient, and low thermal conductivity. Its 2D-crystal structure can be regarded as a natural intergrowth between electronic-conducting Co^{3+}/Co^{4+} hexagonal layers and oxygen deficient Co^{2+}/Co^{3+} rock-salt layers with low thermal conductivity. Their lacunar character suggests a possible anionic conductivity. We took advantage of this model for application as a SOFC cathode material. Additional advantages appear from the good chemical and mechanical adaptability (TEC = $9-10 \times 10^{-6}$ °C^{-1}) with intermediate temperature electrolyte, namely, CGO. The manufactured symmetrical cells show a good electrode/electrolyte adherence, stable after long-time experiments. Our promising preliminary electrochemical tests show a rather low electrode overpotential ($4\Omega\cdot cm^2$) for ~40 μm thick layers with a rather dense microstucture. The porosity and electric performances are improved in the composite with 30 wt % CGO (~1 $\Omega\cdot cm^2$). In general, from polarization experiments versus temperature and oxygen pressure, we found two distinct processes, frequency-separated, that is, HF, charge transfer at the TPB with intrinsic O^{2-} diffusion; LF, gas transfer/oxygen dissociation. This latter is largely fastened in the $CGO/Ca_3Co_4O_{9-\delta}$, reminiscent of the existing but limiting ionic mobility in the single phase of the title compound.

Introduction

Intermediate temperature SOFCs (IT-SOFCs) ideally working in the 500−700 °C range receive considerable attention due to lower running costs, materials compatibility, and long-time durability.[1] Their expected electric conversion efficiency well adapted to stationary applications requires (i) the preservation of high ionic electrolyte performances, (ii) improvement of the catalytic activity with minor electrical losses at the electrodes, and (iii) good cathode/electrolyte/anode chemical and mechanical compatibility along thermal cycling for cell durability. It is generally established that the cathode material becomes one major obstacle while reducing the working temperature.[2] Here the reaction at the so-called three phases boundary (TPB) $^1/_2O_2$ (gas) + $2e^-$ (cathode) $\rightarrow O^{2-}$ (electrolyte) drives the electric performances and is mainly responsible for overpolarization of the fuel cell. Then, the necessity to provide new adapted cathode materials for SOFC has turned out to be one hot topic for the concerned scientific community.[3] This need in such functional materials becomes all the more a priority since the discovery of so-called "colossal" O^{2-} conductivity at the ZrO_2:Y_2O_3 interfaces for epitaxial thin heterogeneous structures.[4] By itself, this result opens wide potentiality toward a significant lowering of the temperature regime until nearly room temperature, and the choice for adapted electrodes becomes crucial.

Standard reported mixed ionic electronic conductor (MIEC) cathode materials for SOFC are commonly 3D-perovskite such as Sr-doped $LaMO_3$ (M = Mn,[5] Co,[6] Fe[3]) or $SmCoO_3$.[7] In particular, the Co-based oxides concerning our purpose have been focused on due to their greater ionic conductivity at intermediate temperature compared to manganites. At the same time, it is known that 3D cobaltites display incompatible aspects in terms

---

*To whom correspondence should be addressed. E-mail: olivier.mentre@ensc-lille.fr.

(1) Steele, B. C. H.; Heinzel, A. *Nature* **2001**, *414*, 345.
(2) Fleig, J. *Annu. Rev. Mater. Res.* **2003**, *33*, 361.
(3) Brandon, N. P.; Skinner, S.; Steele, B. C. H. *Annu. Rev. Mater. Res.* **2003**, *33*, 183.
(4) Garcia-Barriocanal, J.; Rivera-Calzada, A.; Varela, M.; Sefrioui, Z.; Iborra, E.; Leon, C.; Pennycook, S. J.; Santamaria, J. *Science* **2008**, *321*, 676.
(5) (a) Matsuzaki, Y.; Yasuda, I. *Solid State Ionics* **1999**, *126*, 307. (b) Jorgensen, M. J.; Primdahl, S.; Bagger, C.; Mogensen, M. *Solid State Ionics* **2001**, *139*, 1. (c) Kening, S.; Jinhua, P.; Naiqing, Z.; Xinbing, C.; Shen, X.; Derui, Z. *Rare Met.* **2008**, *27*, 278.
(6) (a) Uchida, H.; Arisaka, S.; Watanabe, M. *Electrochem. Solid-State Lett.* **1999**, *2*, 428. (b) Kishimoto, H.; Sakai, N.; Horita, T.; Yamaji, K.; Brito, M. E.; Yokokawa, H. *Solid State Ionics* **2007**, *178*, 1317. (c) Hjalmarsson, P.; Sogaad, M.; Mogensen, M. *Solid State Ionics* **2008**, *179*, 1422.
(7) (a) Fukunaga, H.; Koyama, M.; Takahashi, N.; Wen, C.; Yamada, K. *Solid State Ionics* **2000**, *132*, 279. (b) Tang, Z.; Xie, Y.; Hawthorne, H.; Ghosh, D. *J. Power Sources* **2006**, *157*, 385. (c) Lu, H.; Zhao, B.-Y.; Wu, Y.-J.; Sun, G.; Chen, G.; Hu, K.-A. *Mater. Res. Bull.* **2007**, *42*, 1999.

of (i) chemical reactivity with zirconia electrolyte and (ii) greater thermal expansion coefficient (TEC > 20×10^{-6} °C^{-1} for $La_{0.6}Sr_{0.4}CoO_3$)[8] than those of standard electrolytes, namely, TEC ~ 10×10^{-6} °C^{-1} for YSZ (yttrium stabilized zirconia), CGO (gadolinium doped ceria), and LSGM ($La_{1-x}Sr_xGa_{1-y}Mg_yO_3$). At this point, one possibility to minimize these effects might be candidates by changing the structural type, such as in oxygen deficient double perovskite $LnBaCo_2O_{5+\delta}$,[9] Ruddlesden-popper $(La,Sr)_{n+1}MnO_{3n+1}$,[10] or *Kagomé* lattice containing $YBaCo_4O_{7+\delta}$ materials with versatile oxygen content.[11] These compounds mainly show an increased anionic mobility assorted with encouraging cathode performances, sometimes highlighting the important role of their 2D-characteristics in the electrochemical process. However, the chemical and thermal expansion compatibilities with the electrolyte remain critical problems to overcome.

The present work is dedicated to the investigation of the 2D-$Ca_3Co_4O_{9-\delta}$ (hereafter Ca349) for cathode application for IT-SOFCs. This misfit compound is most known for thermoelectric applications[12] which involve a high figure of merit ZT ($ZT = S^2\sigma T/\kappa$, where S, σ, T, and κ are the Seebeck coefficient, electrical conductivity, absolute temperature, and thermal conductivity, respectively) assorted with an optimal electrical conductivity, reported >100 S/cm from room temperature to 800 °C.[13] It is noteworthy that the misfit structure is built upon sandwiching [CdI_2]-type and rock-salt slabs according to the formula $[CoO_2][Ca_2CoO_{3-\delta}]_{0.62}$, the latter rock-salt layers being oxygen deficient. It is worth recalling that the low thermal conductivity is supposedly due to both the structural modulation and the oxygen vacancies in the rock salt blocks, acting as phonon scatterers. In addition, from the specificities of similar [CoO_2] layers in superconducting sodium−cobalt bronzes hydrates,[14] the layered electronic transport appears strongly efficient and mainly responsible for the electronic specificities of Ca349. From this scheme, Ca349 could also be considered as a natural intergrowth between electronic and O^{2-} conducting units. It makes of this compound an excellent candidate for the SOFC cathode. Here we present our results about chemical stability, thermal expansion, and electrochemical performances of both $Ca_3Co_4O_9$ and the composite 70 wt % $Ca_3Co_4O_9$−30 wt % CGO composite (30CGO). Those materials appear to be suitable and strongly efficient for intermediate temperature applications.

Experimental Section

Polycrystalline Ca349 was synthesized using the conventional solid state reaction. The stoichiometric mixture sample was prepared from reagent grade $CaCO_3$ and Co_3O_4 powders as precursors and calcined at 880 °C for 12 h under air.

For thermal expansion measurements, powder was shaped into pellets by uniaxial pressing at 10 MPa and sintered at 880 °C for 24 h in air, leading to 5 mm in diameter and ~7 mm thick pellets. 30CGO composites have also been prepared adding reagent grade $Ce_{0.9}Gd_{0.1}O_{1.95}$ (Anan Kasei Co. Ltd.). The thermal expansion coefficient (TEC) was measured using a Linseis, L75 dilatometer. The measurements were carried out from 150 to 820 °C in several cycles.

The main stages for ink preparation and electrode deposition have already been presented in a recent study on Ru-pyrochlore cathodes.[15] Briefly, it consists in the addition of 2 wt % dispersant (alkyl ether phosphate acid) to the Ca349 powder and a subsequent ball milling in acetone using zirconia mortar. After air drying at room temperature, 65 wt % of organic binder (terpenoid slurry) was added. Finally, the ink was obtained by mixing again with acetone. The CGO electrolyte pellets, of typically 10−11 mm in diameter and 1.5−2 mm thick after sintering, were formed by uniaxial pressing at 2.5 MPa and sintered at 1200 °C for 2 h in air. Symmetrical cells were obtained by painting/drying the CGO pellets on both sides using the selected ink. Cells are then heated up from room temperature to 500 °C during 12 h and then at 700 °C during 2 h and cooled down to room temperature during 6 h.

XRD analysis of powders and deposited pellets was carried out using a Bruker, D8 diffractometer, Cu Kα radiation. High temperature X-ray diffraction (HT-XRD) was measured for Ca349 powder from 150 to 950 °C using an Anton Paar HTK 1200N chamber under flowing air, ΔT = 25 K. The lattice parameters of the two sublattices were refined using the profile-matching mode available in JANA2006.[16] Here, we used the modulated 4D-composite approach in the X2/m(0, p, 0)s0 super space group, $p \sim 0.62$. The X symbol denotes the 4D (1/2 1/2 0 1/2) centering. Sublattices [CoO_2] and [Ca_2CoO_3] are related by symmetry (for a full crystallographic description, see ref 17).

Impedance spectroscopy measurements were performed using the Solartron, SI 1260 analyzer in the 1.0 mHz−1.0 MHz domain. The imposed signal amplitude during measurements was verified to be low enough (50 mV) for a zero DC polarization current approximation, with respect to the linearity of the electrical response. Gold electrodes were used as current collectors. Measurements were performed at various temperatures and under various oxygen partial pressures as detailed in the concerned section. However, it is noteworthy that we paid a special attention to the stabilization time, necessary to reach equilibrium between each temperature or pO_2 step. Typically

---

(8) Ullmann, H.; Trofimenco, N.; Tietz, F.; Stöver, D.; Ahmad-Khanlou, A. *Solid State Ionics* **2000**, *138*, 79.

(9) (a) Tarankón, A.; Skineer, S. J.; Chater, R. J.; Hernández-Ramírez, F.; Kilner, J. A. *J. Mater. Chem.* **2007**, *17*, 3175. (b) Kim, G.; Wang, S.; Jacobson, A. J.; Reimus, L.; Brodersen, P.; Mims, C. A. *J. Mater. Chem.* **2007**, *17*, 2500. (c) Kim, J. H.; Manthiram, A. *J. Electrochem. Soc.* **2008**, *155*, B385.

(10) Manthiram, A.; Prado, F.; Armstrong, T. *Solid State Ionics* **2002**, *152*, 647.

(11) (a) Karppinen, M.; Yamauchi, H.; Otani, S.; Fjita, T.; Motohashi, T.; Huang, Y. H.; Valkeap, M.; Fjellvg, H. *Chem. Mater.* **2006**, *18*, 490. (b) Tsipis, E. V.; Kharton, V. V.; Frade, J. R. *Solid State Ionics* **2006**, *177*, 1823. (c) Tsipis, E. V.; Khalyavin, D. D.; Shiryaev, S. V.; Redkina, K. S.; Núñez, P. *Mater. Chem. Phys.* **2005**, *92*, 33.

(12) (a) Li, S.; Funahashi, R.; Matsubara, I.; Ueno, K.; Yamada, H. *J. Mater. Chem.* **1999**, *9*, 1659. (b) Limelette, P.; Hardy, V.; Auban-Senzier, P.; Jerome, D.; Flahaut, S.; Hebert, R.; Fresard, Ch. Simon *Phys. Rev. B* **2005**, *71*, 233108-1. (c) Miyazaki, Y. *Solid State Ionics* **2004**, *172*, 463.

(13) Lin, Y. H.; Nan, C. W.; Liu, Y.; Li, J.; Mizokawa, T.; Shen, Z. *J. Am. Ceram. Soc.* **2007**, *90*, 132.

(14) Takada, K.; Sakurai, H.; Takayama-Muromachi, E.; Izumi, F.; Dilanian, R. A.; Sasaki, T. *Nature* **2003**, *422*, 53.

(15) Ehora, G.; Daviero-Minaud, S.; Steil, M. C.; Gengembre, L.; Frére, M.; Bellayer, S.; Mentré, O. *Chem. Mater.* **2008**, *20*, 7425.

(16) Petricek, V.; Dusek, M.; Palatinus, L. *JANA2006, The Crystallographic Computing System*; Institute of Physics: Praha, Czech Republic, 2006.

(17) (a) Grebille, D.; Lambert, S.; Bouree, F.; Petricek, V. *J. Appl. Crystallogr.* **2004**, *37*, 823. (b) Ling, C. D.; Aivazian, K.; Schmid, S.; Jensen, P. *J. Solid State Chem.* **2007**, *180*, 1446.

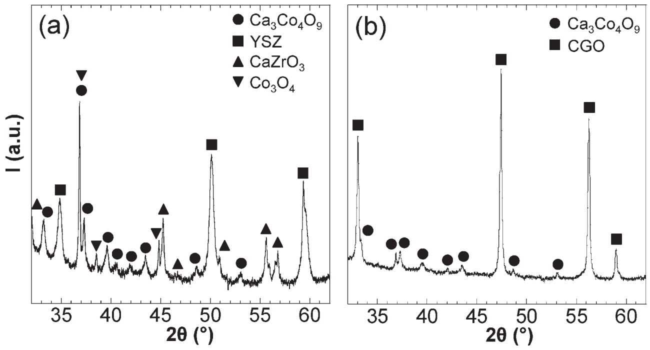

Figure 1. XRD pattern after reactivity tests between $Ca_3Co_4O_{9-\delta}$ and YSZ (a) or CGO (b).

between each temperature step, the stabilization time is more than 4 h, while the pO_2 stabilization is performed overnight. Before each measurement it was checked that the electrochemical response was stable. Here, we defined our own stability criteria based on two successive measurements ($\Delta t \approx 2$ h) of Rp that should not evolve of more than 5%.[15] The impedance spectra are treated and refined using ZView 3.1c.[18]

Scanning electron microscopy (SEM) was performed using a FEG Hitachi Ltd. S-4700 microscope for micrographs of powder grains and cross section of the cells.

Results and Discussion

Chemical and Mechanical Compatibility. The preliminary test for electrode/electrolyte reactivity has been performed considering the 50 wt % Ca349 and 50 wt % YSZ or CGO mixture pelletized under 10 MPa and heated for 100 h at 800 °C. Previous studies have already suggested the incompatibility between zirconia-based electrolyte and cobaltite $La_{1-x}Sr_xCoO_3$ (LSC) or Manganite $La_{1-x}Sr_xMnO_3$ (LSM). It yields the formation of low conductive $La_2Zr_2O_7$ or $SrZrO_3$.[19] In the case of Ca349, the formation of $CaZrO_3$ and Co_3O_4 products was clearly observed and seriously restricts the viability of such an interface. However, as shown on Figure 1, no reaction occurs in the same conditions using CGO which highlights the pertinence of our study. Beside the electrochemical performances, the mechanical electrode/electrolyte compatibility is a necessary attribute for a potential cell. It should protect from superficial cracks which irremediably damage the electric capacity after several cyclings. To our knowledge, the thermal expansion coefficient (TEC) has rarely been reported in the literature for Ca349. It was only measured for doped $Ca_{2.7}Bi_{0.3}Co_4O_9$ to estimate the durability of mounted thermoelectrics p-type $Ca_3Co_4O_9$/n-type$CaMnO_3$ modules, leading to TEC = $8-9 \times 10^{-6}$ °C^{-1} between 100 and 900 °C.[20] Our experimental thermal expansion and related TEC results are shown in Figure 2 for Ca349 and 70 wt % Ca349−30 wt % CGO composite. It yields TEC values of Ca349 between 9 and 10×10^{-6} °C^{-1}. Of course the effect of dilution of 30 wt % CGO

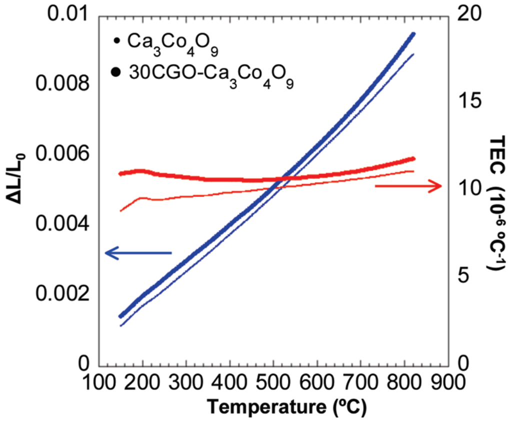

Figure 2. Linear thermal expansion and thermal expansion coefficient of $Ca_3Co_4O_9$ (small filled circles) and 30CGO composite (large filled circles).

slightly shifts this value to $10-11 \times 10^{-6}$ °C^{-1} as expected from the TEC of this latter CGO around $11-12\times 10^{-6}$ °C^{-1} in the same thermal range.[21] As already mentioned in the Introduction, such thermal dilatation coefficients are similar to those of standard electrolytes ($\sim 10\times 10^{-6}$ °C^{-1}) compared to prohibitive values of around 20×10^{-6} °C^{-1} in most of the Co-based 3D-perovskites. Furthermore, this good compatibility is favorable for long-term stability. HT-XRD experiments have been performed to evaluate the anisotropy of the thermal expansion along the distinct crystallographic axes. At this point, we must insist on the particularity of such a layered structure. It is all the more complicated by the incommensurate imbrications of two monoclinic sublattices according to the structural composite approach. They are conventionally called sublattice H, which stands for hexagonal CdI_2-type layers $[CoO_2]$, with axes a, b_H, and c and sublattice RS, for rock salt blocks $[Ca_2CoO_{3-\delta}]$, with parameters a, b_{RS}, and c. The modulation vector along b^* is given by $p = b_H/b_{RS}$. Figure 3 depicts the temperature dependence of the lattice parameters. Their evolutions result from several phenomena reported in the literature, while new insights can be deduced from the comparison between the individual observation of each sublattice. First, it is known that the oxygen nonstoichiometry concerns the rock-salt blocks leading to the chemical formula $[CoO_2]_{1.62}[Ca_2CoO_{3-\delta}]$, where δ changes from 0 to 0.14 depending on the oxygen pressure. Considering a +3.5 value for the cobalt valence in the $[CoO_2]$ layer (as in $Na_xCo_2O_4$ with similar $[CoO_2]$ layers), the mean valence of cobalt in the $[Ca_2CoO_{3-\delta}]$ layer is estimated to be in the range of +2.54 to +2.81.[22] Indeed, as-prepared samples are reported with δ close to zero while heating under air, a progressive oxygen loss, is detected reaching $\delta \sim 0.10$ at 900 °C.[23] Thus, mainly rock salt blocks should become partially reduced on heating. In addition, above 650 °C,

---

(18) *ZView 3.1c*; Scribrer Associates Incorporated: Southern Pines, NC, 2009.

(19) Ralph, J. M.; Rossignol, C.; Kumer, R. *J. Electrochem. Soc.* **2003**, *150*, 1518.

(20) Urata, S.; Funahashi, R.; Mihara, T.; Kosuga, A.; Sodeoka, S.; Tanaka, T. *Int. J. Appl. Ceram. Technol.* **2007**, *4*, 535.

(21) (a) Kharton, V. V.; Kovalevsky, A. V.; Viskup, A. P.; Shaula, A. L.; Figueiredo, F. M.; Naumovich, E. N.; Marques, F. M. B. *Solid State Ionics* **2003**, *160*, 247. (b) Du, Y.; Sammes, N. M.; Tompsett, G. A.; Zhang, D.; Swan, J.; Bowden, M. *J. Electrochem. Soc.* **2003**, *150*, A74.

(22) Shimoyama, J.; Horii, S.; Otzschi, K.; Sano, M.; Kishino, K. *Jpn. J. Appl. Phys.* **2003**, *42*, L194.

(23) Oide, Y.; Miyazaki, Y.; Huang, X. Y.; Kajitani, T. *Proceedings of XXV International Conference on Thermoelectrics* (*ICT '06*), Vienna, Austria, Aug 6−10, 2006; IEEE: New York, 2006; pp 402−405.

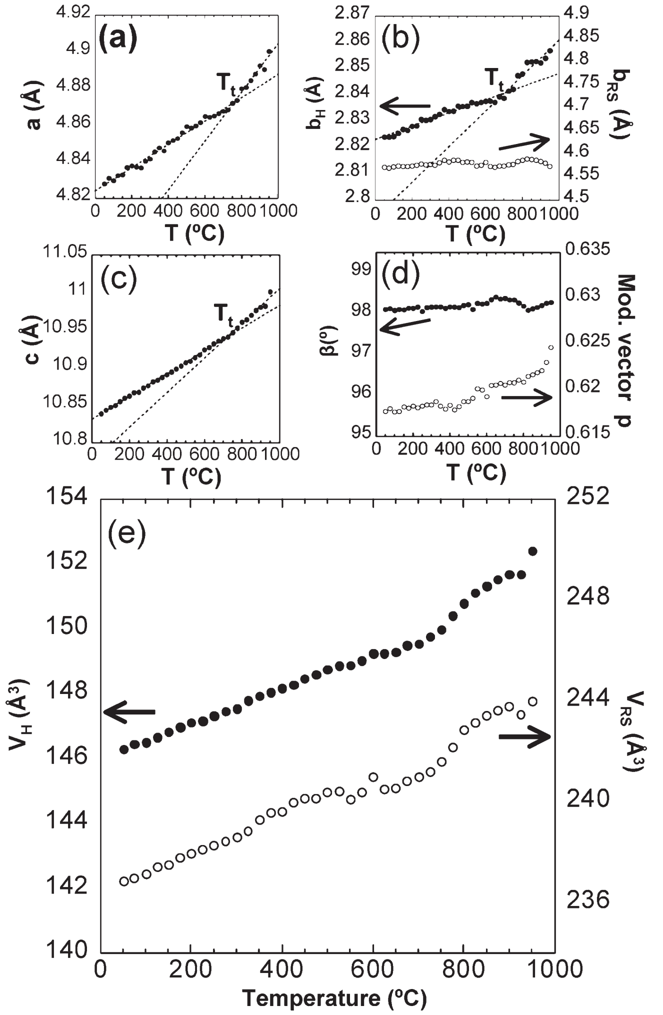

Figure 3. Lattice parameters (a−c) *a*, *b*, and *c*, (d) β and *p*, and (e) volume versus temperature.

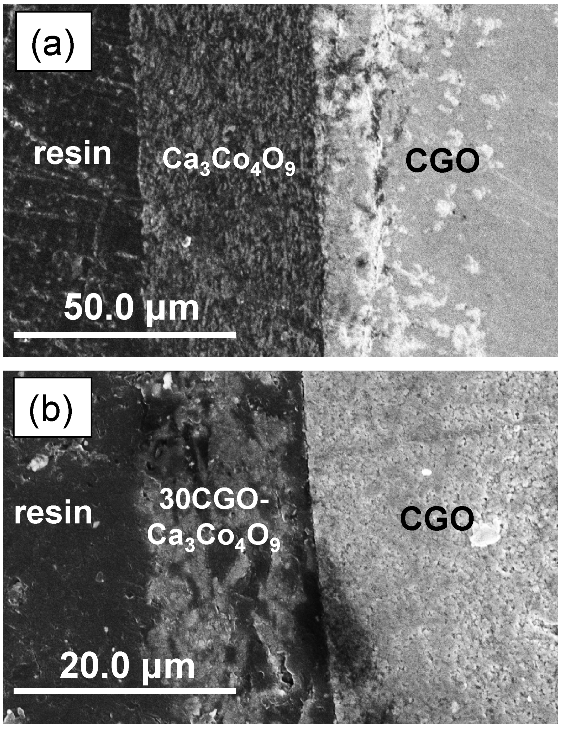

Figure 4. Scanning electron micrographs of cutting cross section of (a) Ca349 and (b) 30CGO deposited on the CGO pellet.

the electrical conductivity shows an abrupt jump. This phenomenon could correspond to a change in the cobalt spin state in H and RS blocks.[23,24] At the upper temperature, Ca349 decomposes into $Ca_3Co_2O_6$ and CoO. Our refined lattice parameters show evidence of a broad transition centered at $T_t \approx 775$ °C, which could picture cobalt spin states mentioned above. At T_t, the slope of the linear dependence of a, b_H, and c increases. However, the less pronounced $b_{RS}(T)$ dependence which is nearly constant suggests that the spin state transition mainly concerns the $Co^{3/4+}$ of the CdI_2-type layers. It is reminiscent of their important role in the electron conduction mechanism.

From Figure 3, the volumic expansion coefficient $\Delta V/(V_0\times\Delta T)$ of sublattices H and RS, in the investigated temperature range, are estimated to be 45×10^{-6} and 32×10^{-6} °C^{-1}, respectively. From the simple volumic expression $V = a\times b\times c\sin\beta$, the TEC anisotropic contributions along the three perpendicular crystallographic axes a, b, and c^* (this latter being perpendicular to the layers) can be developed using $\Delta V/(V_0\times\Delta T) = 1/\Delta T(\Delta a/a_0 + \Delta b/b_0 + \Delta(c^*\sin\beta)/c_0\sin\beta_0) = TEC_a + TEC_b + TEC_{c^*}$. Then, from Figure 3, we calculated the values of these contributions for $\Delta T = 900$ °C.

Sublattice H:

$$45\times10^{-6}(V) = 16\times10^{-6}(a) + 11\times10^{-6}(b_H) + 18\times10^{-6}(c^*)$$

Sublattice RS:

$$34\times10^{-6}(V) = 16\times10^{-6}(a) + 0(b_{RS}) + 18\times10^{-6}(c^*)$$

The following points can now be made:

(i) The difference of TEC along b between the two sublattices is compensated by the increase of the p modulation vector upon heating. It means that their geometrical imbrication along b and the stoichiometric ratio between them (mean formula = $[H]_{1/p}[RS]$) are progressively modified to respect the matching of both lattices. It also involves the creation of defects and constraints on heating/cooling cycles.

(ii) In the RS lattice, one should note that the change in oxygen stoichiometry versus temperature compensates the standard positive thermal expansion, the b_{RS} lattice parameter remaining nearly constant versus temperature. In the opposite, at both sides of T_t, the stoichiometric $[CoO_2]$ layers show a standard thermal expansion.

(iii) By averaging TEC along a, b_H, b_{RS}, and c^*, we found the theoretical TEC $\sim 13\times10^{-6}$ °C^{-1} rather close to the experimental value of $9-10\times10^{-6}$ between 30 and 930 °C. The difference is explained by the compacity of the pellets used

---

(24) Masset, A. C.; Michel, C.; Maignan, A.; Hervieu, M.; Toulemonde, O.; Studer, F.; Raveau, B.; Hejtmanek, J. *Phys. Rev. B* **2000**, *62*, 166.

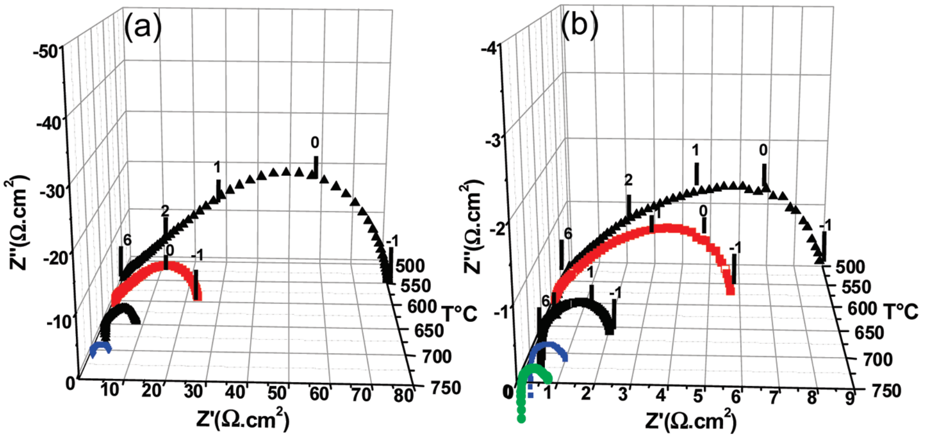

Figure 5. Temperature dependence of impedance spectra of pure Ca349 (a) and 30CGO (b) on air. The characteristic frequencies are indicated by their decimal exponents in Hertz, e.g., −1 for 10^{-1} Hz.

for TEC determination (~80% after TEC measurement). Of course, concerning the technical aspect involved in porous electrode layers, the effective experimental TEC prevails.

(iv) The dilatation appears slightly anisotropic by comparing the components along *a*, *b* (average of H and RS contributions → 5.5×10^{-6} °C^{-1}), and *c**. It mainly shows lowest and greatest expansion along *b* and *c**, respectively. However, the SEM micrographs discussed below show plaquette-like shaped crystallites, in probable relation with the layered structure of Ca349. The accommodation of large/weak TEC with short/long dimensions of the crystals is expected to reduce the disagreements possibly due to anisotropic expansion effects.

Electrochemical Characterization. To optimize the microstructure of the electrode, we have followed the grain size evolution in function of grinding time. The powders were mixed with acetone and ground by ball-milling (zirconia mortar at 700 t/min) with various duration. The grain size was determined by SEM micrographs. Figure S1 of the Supporting Information shows the grains before ball milling and after 9, 12, and 24 h grinding times. No significant decrease of the grain size was observed before 12 h, the particle size being in the range of 1.5−4 μm. However, an obvious grain size reduction after 24 h had been found, leading to 0.5−1 μm particles. This preliminary grinding step was adopted for Ca349 and CGO/Ca349 composite. By comparison with others colbaltite cathodes like LSC or our current results on other cobaltites such as $Ba_2Co_9O_{14}$,[25] the CGO/Ca349 adherence is good, leading to homogeneous layers typically 15−30 μm thick (Figure 4).

The good adhesion at the interface is perceptible through the absence of cracks on the surface (see Supporting Information Figure S2). However, after electrode sintering, the porosity seems reduced according to the SEM micrographs shown on the Figure 4a. This grain aggregation is a major obstacle to overcome in our future works. The XRD analysis of the deposited electrode layer shows no evidence of phase degradation after the sintering stage. For comparison purposes, pure Ca349 and 30CGO cathodes were prepared using the same method as described before. The cathode performance of Ca349 and 30CGO in a symmetrical cell configuration was investigated via AC impedance spectroscopy under air and various oxygen atmospheres. The measurements were carried out on heating by steps of 50 °C from 540 to 760 °C. In addition, electrochemical measurements were also performed at various pO_2 values ranging from 3×10^{-5} to 1 atm. The oxygen partial pressure was monitored by mixing O_2 and N_2 by means of an electrochemical pump and an oxygen gauge.

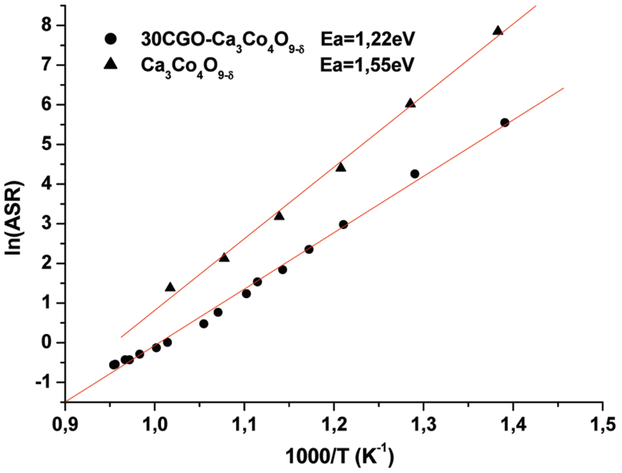

Figure 6. Arrhenius plots of total polarization resistance and calculated activation energies of Ca349 (filled triangle) and 30CGO (filled circle) cathodes deposited on the CGO pellet in air.

Pure Ca349. The Nyquist plot for the Ca349 electrode under air is shown in Figure 5a as a function of the temperature. The impedance spectra are characterized by a single impedance arc intercepting the real axis at approximately 45° in the high-frequency domain characteristic of a Warburg or Gerischer impedance circuit. The former was preferred to a Gerischer-impedance leading to best refinements, see Supporting Information, Figure S3, but it involves solid state anionic diffusion

---

(25) Ehora, G.; Daviero-Minaud, S.; Colmont, M.; André, G.; Mentré, O. *Chem. Mater.* **2007**, *19*, 2180.

Table 1. Calculated Normalized Polarization Resistance, *m*-Value, and Activation Energy in Ca349

	normalized polarization resistance ($\Omega \cdot cm^2$)											
	700 °C			600 °C			500 °C			activation energy (eV)		
oxygen partial pressure (atm)	W_R	R2	total ASR	W_R	R2	total ASR	W_R	R2	total ASR	W_R	R2	total ASR
1	2.34	2.60	4.94	161.4	21.0	37.4	10.4	506	516	1.43	1.71	1.51
2.1×10^{-1}	1.29	2.72	4.00	13.1	11.4	24.5	297	71.66	369	1.69	1.28	1.55
2×10^{-3}	11.2	6.40	17.6	47.2	21.3	68.6	128	674	802	0.78	1.53	1.25
3×10^{-4}	24.5	46.1	70.6	141	65.9	207	360	1541	1901	0.86	1.17	1.08
7×10^{-5}	51.1	148	199	365	408	773	511	4064	4575	0.72	1.09	1.02
m-value	0.42	0.58		0.40	0.40		0.42	0.49				

that will be discussed below. It is associated with a vertical negative drop, being related to the inductance *L* attributed to high-frequency artifacts arising from the measurement apparatus. The intercept of the electrode impedance on the real axis R1 represents the overall ohmic resistance, namely, the electrode ⊕ CGO pellet ⊕ lead wire resistances. However, up to 400 °C no impedance contributions of the CGO−electrolyte and grain boundaries are observed. As a result of the symmetrical cell geometry, the area specific resistance (ASR) was calculated from the total polarization resistance Rp and electrode surface area *S* using the following formula: $ASR = (Rp \times S)/2$. ASR(*T*) obeys an Arrhenius behavior with typical values from 4 to 400 $\Omega \cdot cm^2$ between 700 and 500 °C, smaller than the pure LSM cathode ($\sim 30\ \Omega \cdot cm^2$)[26] but higher than the LSCF one ($\sim 0.5\ \Omega \cdot cm^2$)[19] at the same temperature. The activation energy value is Ea = 1.55 eV (Figure 6 and Table 1) to be compared with the 1.6 eV of the LSM cathode and the 1−1.6 eV of the LSCF. As a matter of fact, taking into account the preliminary character of our study, these rather low values emphasize the interest for developing this cobaltite.

The electrode reaction involves several interplaying processes and/or limiting mechanisms: (i) oxygen reduction/charge transfer at the current collector/electrode interface and electrode/electrolyte interfaces, (ii) oxygen exchange at the electrode surface, (iii) bulk and surface diffusion of oxygen species, and (iv) gas phase diffusion[26] imply the deconvolution of the impedance spectra into elementary semicircles fitted by corresponding equivalent circuits. For Ca349, the impedance arc deconvolution shows two overlapping depress circles leading to the equivalent circuit of Figure 7. Then, the electrode reaction involves a Warburg element W_S (short circuit terminus) at high frequency response and R2 associated with a constant phase element CPE (low frequency response). That equivalent circuit was considered for all investigations, including T and pO_2 effects and modification of the electrode by CGO-adding, see Tables 1 and 2. The impedance of CPE can be express as $Z = 1/[B(j\omega)^{\alpha}]$ where *B* is a constant independent of the frequency, ω is the angular frequency, and α an exponential term. For $\alpha = 1$, CPE represents an ideal capacitance *C*.

The equivalent circuit itself assorted with the frequency range for the two contributions is nearly similar to that observed for $Sr_{1-x}La_xCo_{0.8}Fe_{0.2}O_{3-\delta}$ (LSCF) deposited on CGO. [27] This latter is recognized as a MIEC above 600 °C[28] and is a promising cathode material, due to large oxygen fluxes expected from its important O^{2-} conductivity. From general features and on the basis of this latter work, the high frequency arc (fitted here by the W_S element) may be associated to the transfer process at the electrode/electrolyte interface. For LSCF, the use of a Warburg circuit has been interpreted as a finite length ionic diffusion. In the absence of experimental evidence for MIEC in Ca349, we have to carefully analyze the HF domain, but an identical phenomenon is plausible taking into account the ideal O^{2-} diffusion paths in the oxygen deficient rocksalt layers. The low frequency arc (fitted here by R2//CPE) can be ascribed to slower mechanisms related to the oxygen diffusion process. It includes the adsorption−desorption of oxygen gas, oxygen diffusion at the gas/cathode interface, and the surface diffusion of the intermediate oxygen species. The absence of any additional high frequency semicircle on experimental impedance diagrams, even when lowering the temperature, can evidence a sufficiently fast charge transfer process occurring at the current collector/electrode and electrode/electrolyte interfaces.[29]

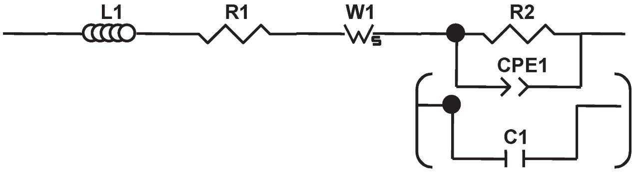

Figure 7. Equivalent circuit used to fit the impedance spectra. Parenthetical reference (capacitor C) is applied according to measurement condition.

Under air, the comparison between W_R (resistivity part of W_S) and R2 for Ca349 shows similar order of magnitude versus temperature, reminiscent of at least two distinct electrochemical processes. As expected, the effect of reducing pO_2 emphasizes the HF and LF circles separation (Figure 8a), but mostly influences R2, in agreement with the driving limitation by the gas/cathode exchange kinetics. It is remarkable that from air ($pO_2 = 0.2$ atm) to oxygen ($pO_2 = 1$) the ASR value increases in the full

---

(26) (a) Liu, M. *J. Electrochem. Soc.* **1998**, *145*, 142. (b) Adler, S. B.; Lane, J. A.; Steele, B. C. H. *J. Electrochem. Soc.* **1996**, *143*, 3554.

(27) Grunbaum, N.; Dessemond, L.; Fouletier, J.; Prado, F.; Caneiro, A. *Solid State Ionics* **2006**, *177*, 907.

(28) Mantzavinos, D.; Hartley, A.; Mercalfe, I. S.; Sahibzada, M. *Solid State Ionics* **2000**, *134*, 103.

(29) (a) Adler, S. B. *Solid State Ionics* **1998**, *111*, 125. (b) Imanishi, N.; Matsumura, T.; Sumiya, Y.; Yoshimura, K.; Hirano, A.; Takeda, Y.; Mori, D.; Kanno, R. *Solid State Ionics* **2004**, *174*, 245.

Table 2. Calculated Normalized Polarization Resistance, *m*-Value, and Activation Energy in 30CGO

oxygen partial pressure (atm)	normalized polarization resistance (Ω·cm^2)												activation energy (eV)		
	760 °C			700 °C			600 °C			540 °C					
	W_R	R2	total ASR	W_R	R2	total ASR	W_R	R2	total ASR	W_R	R2	total ASR	W_R	R2	total ASR
1	0.36		0.36	0.71		0.71	5.21		5.21	19.9		19.9	1.35		1.35
2.1×10^{-1}	1.00	0.05	1.05	1.39	0.02	1.42	6.83	0.86	7.68	17.0	4.48	21.5	1.11	1.88	1.22
1.2×10^{-3}	2.40	9.15	11.6	4.00	11.7	15.6	13.0	12.0	25.0	26.4	20.5	46.8	0.80	0.22	0.44
1.4×10^{-4}	6.16	46.6	52.7	6.23	60.9	67.1	19.5	81.0	100	40.4	128	168	0.67	0.31	0.37
3.7×10^{-5}	120	1280	1399	178	1906	2084	431	3539	3970	622	5024	5646	0.56	0.45	0.46
m-value	0.26	0.94		0.25	1.00		0.14	0.85		0.11	0.85				

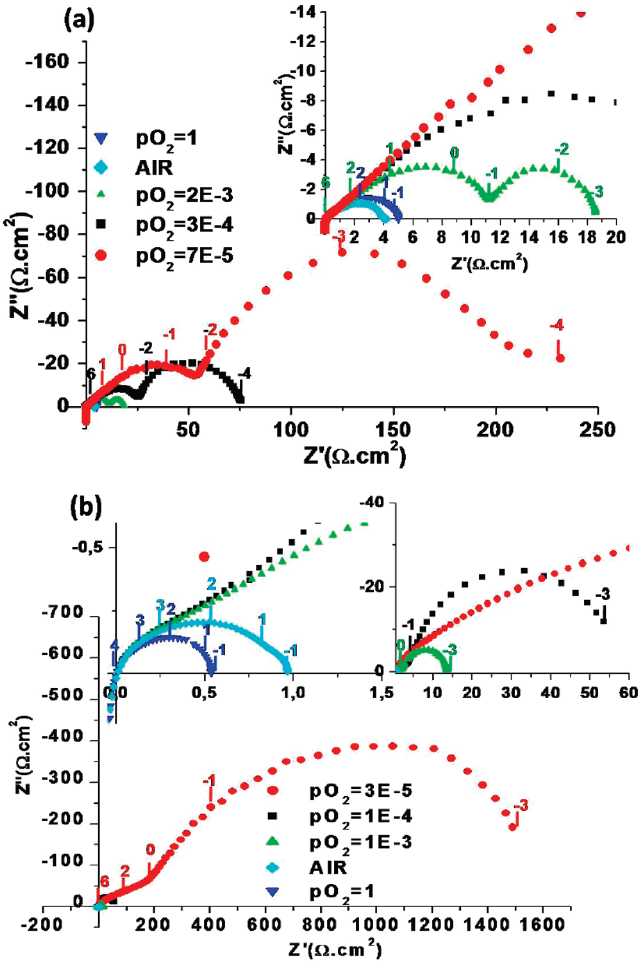

Figure 8. Oxygen partial pressure dependence of impedance spectra for Ca349 (a) and 30CGO (b) at 700 °C. The insets show various levels of zoom.

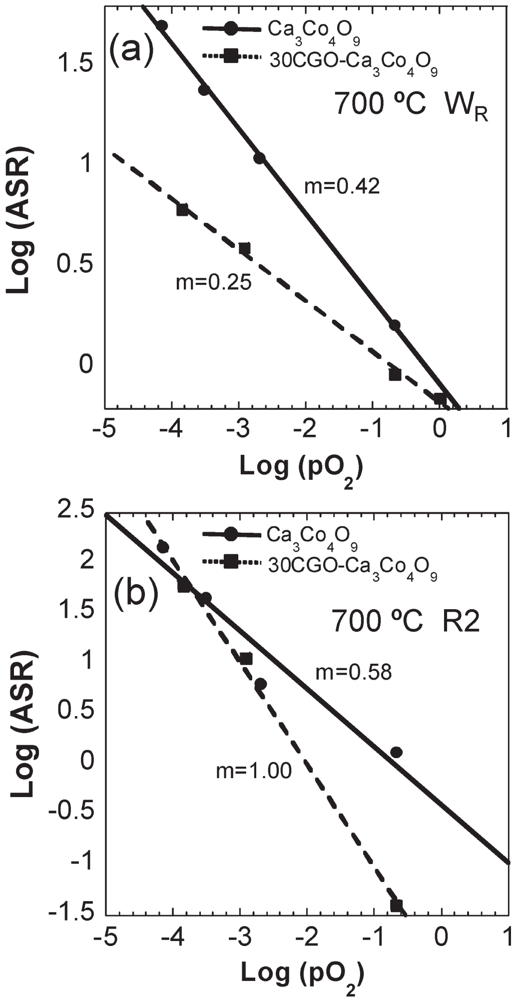

Figure 9. pO_2 dependence of ASR and calculated *m*-values at 700 °C of charge transfer resistance (a) WR and (b) diffusion resistance R2.

investigated temperature range. This rather rare phenomenon should be the consequence of a sensitive oxidation of rock salt layers toward a greater Co^{III}/Co^{II} ratio. The deterioration of the electrochemical performances under high pO_2 is under investigation but is an additional clue for the participation of intrinsic ionic mobility in Ca349 that would strongly depend on the concentration in oxygen vacancies.

The analysis of the dependence on pO_2 can qualitatively be expressed in terms of the phenomenon associated with each subcircuit. A possible distinction between elementary mechanisms follows from the evaluation value of the reaction order *m* according to $R_{el} \propto (pO_2)^{-m}$:[30]

- Reaction involving molecular oxygen concentration such as gaseous diffusions of oxygen molecules ($m \sim 1$)
- O_2 dissociation reaction including adsorption/desorption and reduction ($m \sim 1/2$)
- Surface exchange process ($m \sim 1/3$)
- Charge transfer at the triple phase boundaries (TPBs), ionic conductivity for MIEC ($m \sim 1/4$).

The logarithmic relation between W_R/R_2 and $p(O_2)$ is shown on the Figure 9 for Ca349 at 700 °C. We found

---

(30) (a) Takeda, Y.; Kanno, R.; Noda, M.; Tomida, Y.; Yamamoto, O. *J. Electrochem. Soc.* **1987**, *134*, 2656. (b) Siebert, E.; Hammouche, A.; Kleitz, M. *Electrochim. Acta* **1995**, *40*, 1741. (c) Mizusaki, J.; Amano, K.; Yamauchi, S.; Fueki, K. *Solid State Ionics* **1987**, *22*, 313.

$m_{R2} = 0.58$ which denotes a significant influence of the working oxygen concentration, in possible relation with the rather dense microstructure and the subsequent oxygen gas dissociation as the limiting step. At least, the oxygen deficient rock salt blocks assorted with the electronic conductivity of CoO_2 layers appears as a serious asset for intrinsic electro-catalytic properties of Ca349, but it should be limited by the oxygen vacancies concentration.[23] From $m_{WR} = 0.42$, we can suppose similar limitations for oxygen reduction and diffusion at the electrode/electrolyte interface. In the case of cathodes with mixed iono-electronic conductivity, the whole electrode/electrolyte contact area is used for O^{2-} transfer. It is in agreement with important decreasing of the LF part magnitude with pO_2 increase, while the influence on the HF contribution is less drastic, see Figure 8a. However, R2 does not drop to zero under oxygen partial pressure, indicating a limitation for gas phase dissociation. The main reason for this will be clarified in the next section. Finally, from the SEM cross sectional views of Figure 4, it follows that the relatively dense and thick Ca349 texture could be largely responsible for the resistant phenomena (HF and LF) detailed above.

Effect of CGO Adding. It is known that the development of a series of new cathodes by mixing the ionic conducting phase results in a significant improvement on the electrochemical properties. In the case of $Ba_{0.5}Sr_{0.5}Co_{0.6}Fe_{0.4}O_{3-\delta}$(BSCF)/$Ce_{0.8}Sm_{0.2}O_{1.9}$, best performances have been obtained for a ratio of 30 wt %.[31] We also found optimized behavior for 70 wt % $Ba_2Co_9O_{14}$[25] 30 wt % CGO in very recent investigation on new cathode materials. This ratio has been selected in our study. It is obvious from the Figure 5b that the ASR is significantly reduced compared to pure Ca349, leading to $1-20\ \Omega\cdot cm^2$ between 760 and 540 °C. The activation energy of the Arrhenius behavior, Ea = 1.35 eV, is less significantly minored, Figure 6, Table 2. No reaction between CGO and Ca349 was detected by XRD after the electrochemical tests.

Two major reasons could explain the positive effect of CGO adding: the reducing of the thermal expansion mismatch problem and improvement of the electrolyte/electrode interfacial front. However, as already discussed, this effect should be minor, taking into account the dilatation adaptability between CGO and Ca349. Then, the important role of CGO-adding should mostly concern the increase of both TPB concentration by creation of strongly efficient O^{2-} diffusion paths in the composite electrode and an increase of the porosity as shown in Figure 4b. The fit reveals that the ohmic overpotential due to both R_2 (better O^{2-} diffusion) and W_R (higher TPB concentration) is improved (Table 2). At 700 and 760 °C, we found m_{R2} of ~1. This maximal pO_2 dependence clearly indicates the efficient function of the added CGO for O^{2-} mobility, since the contribution to the overpotential corresponding to gas-oxygen absorption and diffusion in the porous solid almost vanishes in air and was not observed in the oxygen atmosphere (R2-0), Figure 8b. As a consequence, as expected for real MIECs, m_{WR} is found to be equal to 1/4, the characteristic value for charge transfer at the TPB and ionic diffusion. Indeed, the relatively low resistance associated with these phenomena as soon as 650 °C is promising.

At this point the very good stability observed for Ca349 and 30CGO cathodes must be mentioned. The impedance measurements done after going back to air atmosphere, after several temperatures and pO_2 cycling, show no modifications of the cell ohmic resistance (Figure S4, Supporting Information).

From these results, by comparison between the two electrodes, it is clear that one limitation associated to Ca349 results from restrained O^{2-} diffusion that enhances the importance of the microstructure through an improvement of TPB concentration. At least this primary investigation seems to indicate that an intrinsic ionic mobility exists in Ca349, in agreement with the best impedance fitting using a Warburg circuit, since mean ASR values are small and gas (LF)/solid (HF) contributions are not clearly separated in air. The microstructural features are hardly comparable between pure Ca349 and the composite, the latter appearing more porous. That effect probably plays an important role on the better properties of the composite cathode.

Concluding remarks

We have investigated the 2D-$Ca_3Co_4O_{9-\delta}$ misfit compound as a possible cathode material for IT-SOFC. Its experimental thermal expansion, between 9 and 10×10^{-6} $°C^{-1}$ for pure Ca349, closed to the TEC of CGO ($11-12\times10^{-6}\ °C^{-1}$) allowed a very good mechanical compatibility at the electrolyte/electrode interface, differently from the Co-based 3D-perovskite cathode with prohibitive TEC values of around $20\times10^{-6}\ °C^{-1}$. Furthermore, the mechanical properties are assorted with an excellent chemical compatibility with CGO which is favorable to long time stability, confirmed by several air impedance measurements without any modifications after long temperature and pO_2 cycling. The investigation of the electrochemical properties showed promising values of the ASR for the $Ca_3Co_4O_{9-\delta}$ cathode comparable with other conventional cathode materials. Furthermore, the 30CGO composite shows an improvement of the cathode reaction, by promoting the O^{2-} diffusion. However, a certain amount of intrinsic ionic diffusion seems to exist in the pure compound. Its improvement in Ca349 should be envisaged in further aliovalent substitution of Ca^{2+}or $Co^{2+/3+}$ in the rock-salt blocks. It is remarkable that, at this point, both the thickness and porosity appears rather limited for cathode performances. Efforts are currently under investigation to improve theses features by both the optimization of the ideal grain size and/or by using porous agents such as cellulose in the deposition stage.

Supporting Information Available: SEM micrographs, fit of Ca349 at 700 °C and 600 °C under air using a HF Warburg and Gerisher circuits, and cell ohmic resistances (PDF). This material is available free of charge via the Internet at http://pubs.acs.org.

---

(31) Li, S. Y.; Lu, Z.; Wei, B.; Huang, X. Q.; Miao, J. P.; Liu, Z. G.; Su, W. H. *J. Alloys Compd.* **2008**, *448*, 116.